JOURNAL OF THERMOPHYSICS AND HEAT TRANSFER
Vol. 21, No. 4, October–December 2007

Subtranscritical and Supercritical Properties for $LO_2 - CH_4$ at 15 MPa

A. Minotti* and C. Bruno†
University of Rome "La Sapienza," 00184 Rome, Italy

DOI: 10.2514/1.31051

Future launchers will use rocket propulsion systems burning CH_4/LO_2 at high chamber pressure, and so it is useful to analyze the thermophysical properties of these species and their combustion products at these conditions. High-pressure (real-gas) effects significantly modify combustion regimes, for instance, the propellants *Re* injected near the critical temperature, and so to simulate mixing and combustion processes in subtranscritical regimes high-pressure effects must be described. This paper analyzes the compressibility factors of CH_4, O_2, CO_2, and H_2O at a pressure of 15 MPa and calculates the difference between ideal- and real-gas thermophysical properties for these species in the range of temperature in which experimental data are available. Finally, the paper describes thermophysical properties at typical liquid rocket engine combustion chamber conditions ($100 < T < 6000$ K, 15 MPa) by polynomial fits. As there are no experimental data at high temperatures, theories are necessary to predict properties at temperatures different from the experimental ones: thus, low-temperature experimental data (National Institute of Standards and Technology tables) are used in conjunction with predictions obtained with the Lee–Kesler equation of state (for density and isobaric specific heat) and with the Chung et al. method (for viscosity and thermal conductivity). This paper will try to clarify the impact of subtrans–supercritical parameters on mixing and combustion in future liquid rocket engines.

Nomenclature

Superscripts

0	=	ideal behavior
r	=	residual behavior

Subscripts

m	=	mixture
c	=	value at critical point
r	=	reduced value

Introduction

AMONG proposed future liquid-rocket-engine-powered launchers are systems using CH4 and LO2 propellants. The injection pressure will be supercritical for both species while the injection temperature will be supercritical for CH4 and subcritical for LO2 [1–5]. To predict performance and help in the design of such propulsion systems, it is mandatory to study the thermophysical properties of these species and their products at representative liquid rocket engine (LRE) conditions. Modeling high-pressure mixing and combustion involves several interconnected physical processes that increase the complexity of predicting injector and combustion behavior.

Close to their critical point, substances exhibit large variations in thermodynamic as well as transport properties that may dramatically affect mixing and combustion; even when one of the propellants, typically oxygen, is injected, liquid, high-heating rates inside the injector may raise its temperature above critical.

Received 15 March 2007; revision received 5 June 2007; accepted for publication 10 June 2007.

*Ph.D., Department of Mechanics and Aeronautics; angelominotti@inwind.it.

†Professor, Department of Mechanics and Aeronautics; Claudio.Bruno@uniroma1.it. Associate Fellow AIAA.

For these reasons, using ideal-gas equation of state may lead to erroneous results, and the same is true when using low-pressure transport properties.

The criterion to verify whether a gas is ideal or not is based on the compressibility factor *Z*:

$$Z = \frac{PV}{RT} \tag{1}$$

For an ideal gas, $Z = 1.0$. For real gases, *Z* is usually less than one, except at high-reduced temperature and pressure. In fact, in certain cases, Eq. (1) can also be used to define *Z* for a liquid. The prediction of all thermodynamic properties depend on the equation of state chosen. Thus, appropriate equations of state (EOS), and methods to determine transport properties must be provided. Because in modeling high-pressure combustion often the regime is transcritical, it is desirable to have an equation of state capable of predicting the pressure, volume, temperature (PVT) behavior of both liquid and gas states. Ideally, such equation should predict thermodynamic properties accurately while being computationally simple. The same consideration applies to methods predicting transport properties.

At the moment, there is no widespread knowledge of the quantitative difference between ideal- and real-gas behavior, and so it is possible to think that, to a first approximation, errors caused by using ideal-gas properties may be of the same order as the numerical one: in fact, this is absolutely false, as shown in what follows.

Thus, the goals of this work are to quantify the thermophysical properties differences between ideal and real gas for species of importance in LRE combustion simulations in terms of *Z*, and to describe their thermophysical properties in a range of temperature from subcritical to ideal gas by providing polynomial fits of these properties easily to implement in computational fluid dynamics (CFD) codes. In pursuing these goals, experimental results are available only in a narrower range of temperature than that of interest ($100 < T < 6000$ K). Hence, the present effort has focused on the "best" theory to use at temperatures higher than the highest experimentally available. Several theories have been analyzed [6] and compared [7]; what follows reports results obtained for density, isobaric heat capacity, viscosity, and thermal conductivity for O_2, CH_4, CO_2, and H_2O species at 15 MPa and $100 < T < 6000$ K.

Table 1 Properties

	T_c, K	P_c, bar	V_c, cm^3/mol	Acentric factor, ω
CH_4	190.4	46.0	99.2	0.0086
O_2	154.6	50.4	77.4	0.0222
CO_2	304.1	73.8	93.9	0.22394
H_2O	647.3	221.2	65.1	0.3443

Compressibility Factor *Z*

The compressibility factor measures the effect of pressure and temperature on the density of the fluid: if $Z > 1$ it means that the effect of pressure is higher than that of temperature; if $Z < 1$, the opposite is true. When $Z = 1$, the two contributes are equal and the gas is defined as ideal, this occurs at temperatures far from the critical point. Table 1 shows the properties for the species analyzed. The Z factor of these at pressure 15 MPa and in the experimentally available range of temperature is reported in Figs. 1–4.

In a wide range of temperatures around the critical point, Z is always less than one. Typical values of Z around the critical point is $0.3/0.6$, slowly growing with T and reaching and exceeding unity; only H_2O has a minimum, for temperatures less than the critical one, at 0.1 and this because the H_2O critical pressure is higher than 15 MPa.

The consequences of Z behavior on density, isobaric specific heat, and viscosity are reported next [7]. Figures 5–12 show a comparison between ideal- and real-gas density in the range of temperatures for which experimental data are available and the corresponding percentage differences.

Figures 6, 8, 10, and 12 report percentage density differences with respect to ideal gas near the critical temperature. They are about 107% for CH_4, about 124% for O_2, about 227% for CO_2, and about 77% for H_2O.

Even though these differences reduce at higher temperatures, they remain higher than 5% (a reasonable value below which real-gas effects might be neglected) in almost the entire range of temperature of interest to LRE. Table 2 shows the temperature above which the density difference is less than 5%.

Figures 13–20 show the real–ideal isobaric specific heat comparisons and the corresponding percentage differences (ideal isobaric specific heats are calculated with the polynomials used in the NASA CEA400 software [8–11]).

Figures 14, 16, 18, and 20 report C_p percentage differences with respect to ideal gas near the critical temperature. They are about 90% for CH_4, about 114% for O_2, about 248% for CO_2, and about 150% for H_2O; these values are not so different from the corresponding ones about density.

Even though these differences reduce at higher temperatures, they remain higher than 5% (a reasonable value below which real-gas effects might be neglected) in almost the entire range of temperature of interest to LRE. Table 3 shows the temperature above which the density difference is less than 5%.

Figures 21–28 show real–ideal viscosity comparisons, report viscosity comparisons (ideal-gas viscosity, calculated with the Sutherland theory [12]) and the corresponding percentage

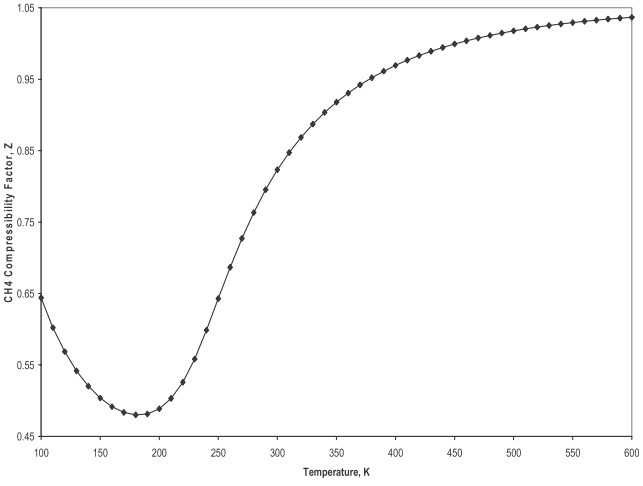

Fig. 1 CH_4, compressibility factor at 15 MPa.

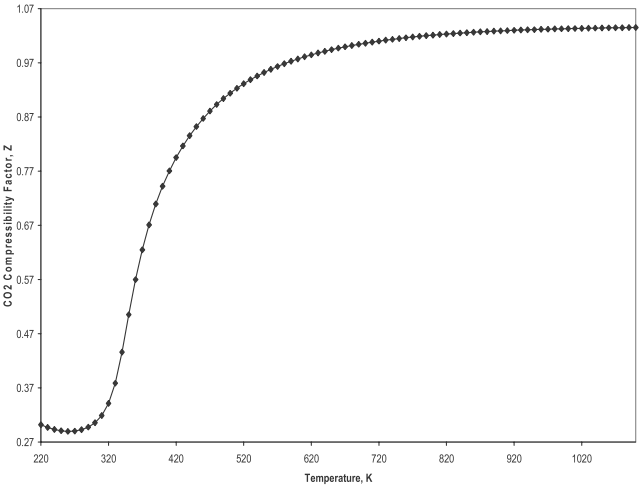

Fig. 3 CO_2, compressibility factor at 15 MPa.

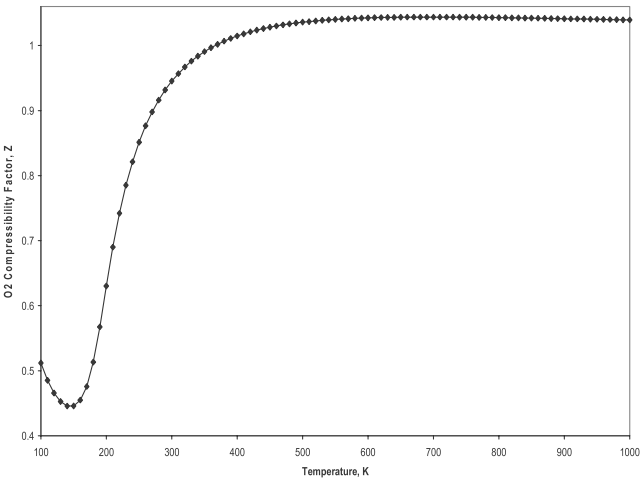

Fig. 2 O_2, compressibility factor at 15 MPa.

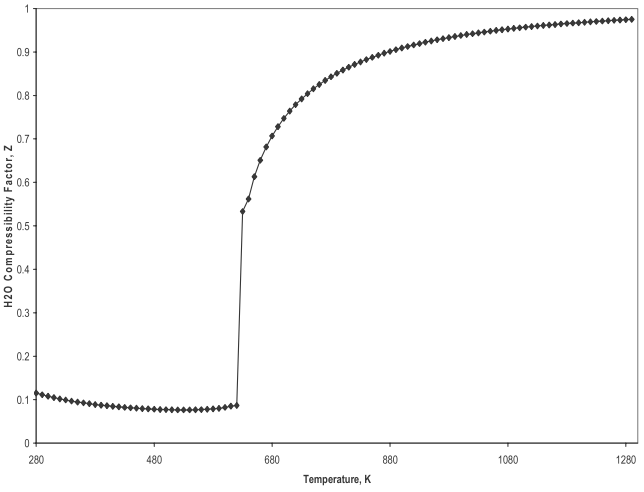

Fig. 4 H_2O, compressibility factor at 15 MPa.

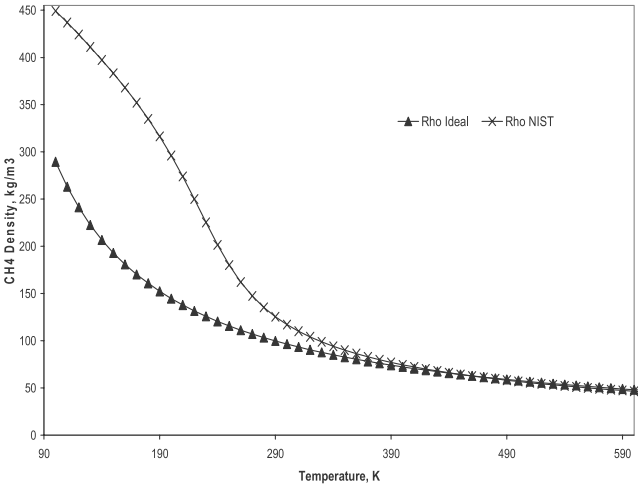

Fig. 5 CH_4, density comparison at 15 MPa.

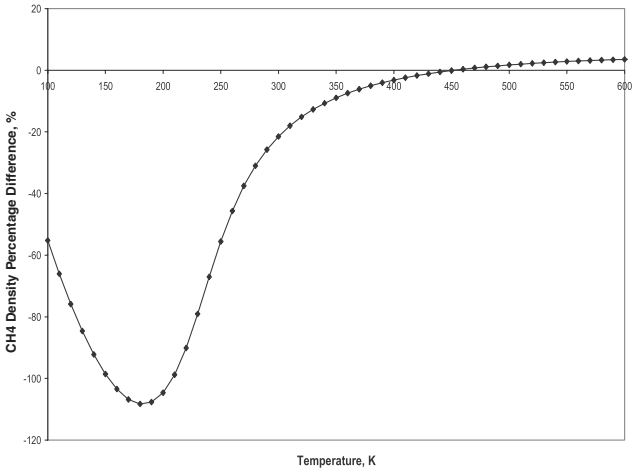

Fig. 6 CH_4, density % difference at 15 MPa.

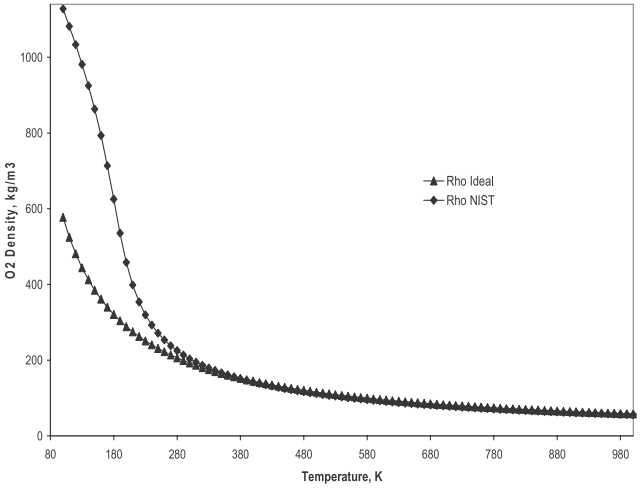

Fig. 7 O_2, density comparison at 15 MPa.

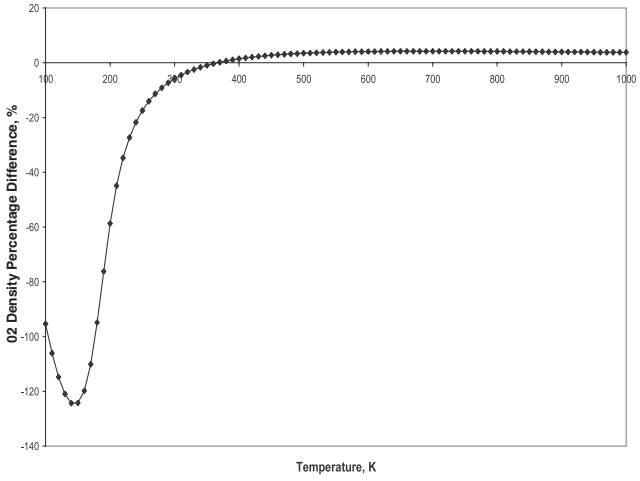

Fig. 8 O_2, density % difference at 15 MPa.

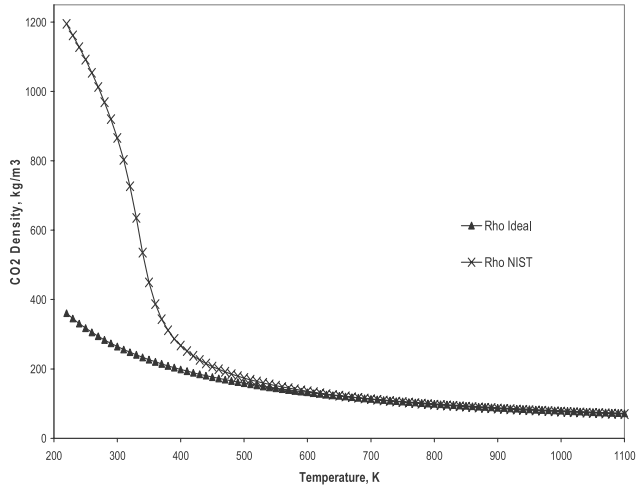

Fig. 9 CO_2, density comparison at 15 MPa.

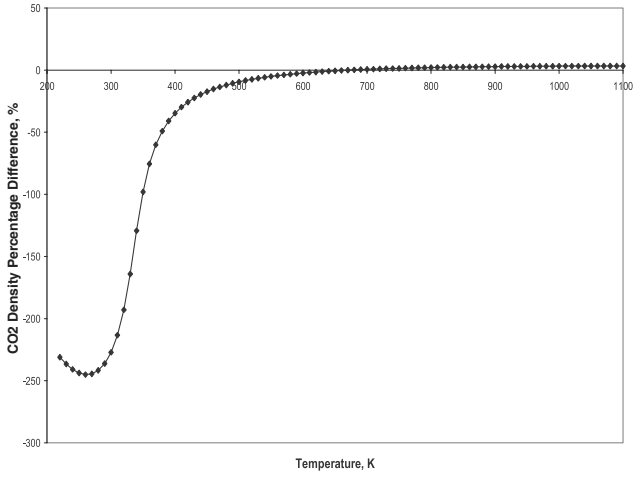

Fig. 10 CO_2, density % difference at 15 MPa.

differences. Therefore, around the critical temperature, the viscosity percentage differences are about 650% for O_2, about 170% for CH_4, about 300% for CO_2, and about 80% for H_2O.

For this, property differences remain higher than 5% in almost the entire range of temperature (see Table 4).

The conclusion is that assuming ideal-gas properties at transcritical and supercritical conditions causes significant errors. For instance (everything else being the same), near the critical temperature, real-gas behavior predicts Reynolds numbers much lower using ideal gas. Similarly, Prandtl numbers will be different and maximum temperature will be lower than the one obtained using

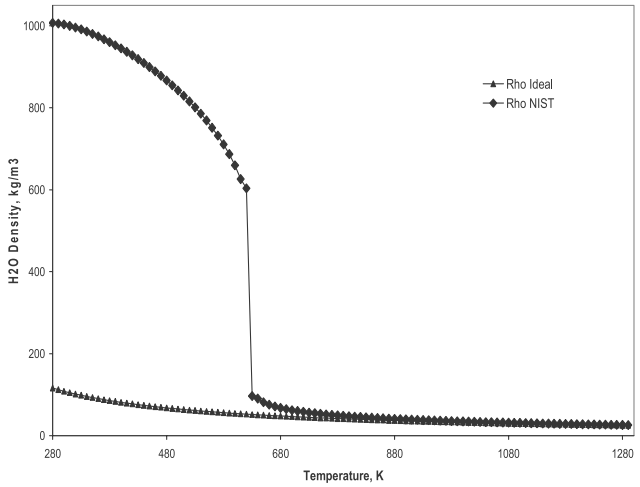

Fig. 11 H_2O, density comparison at 15 MPa.

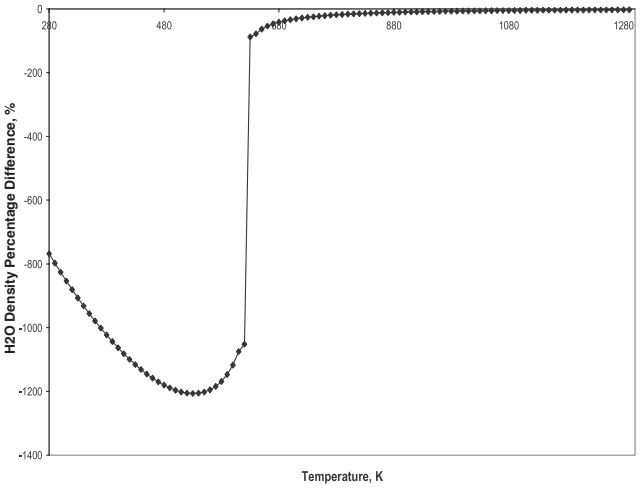

Fig. 12 H_2O, density % difference at 15 MPa.

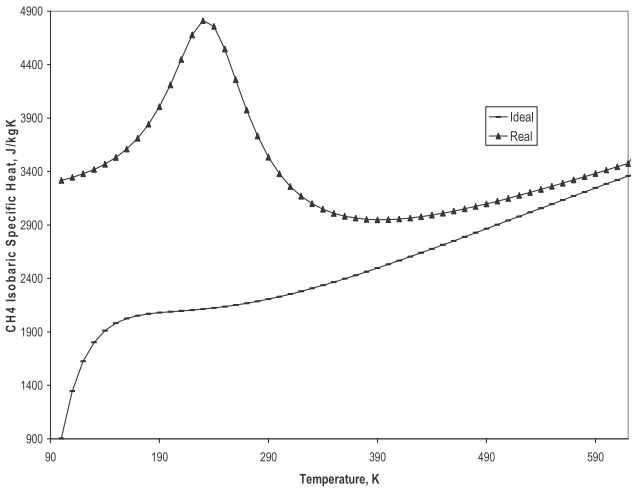

Fig. 13 CH_4, C_p comparison at 15 MPa.

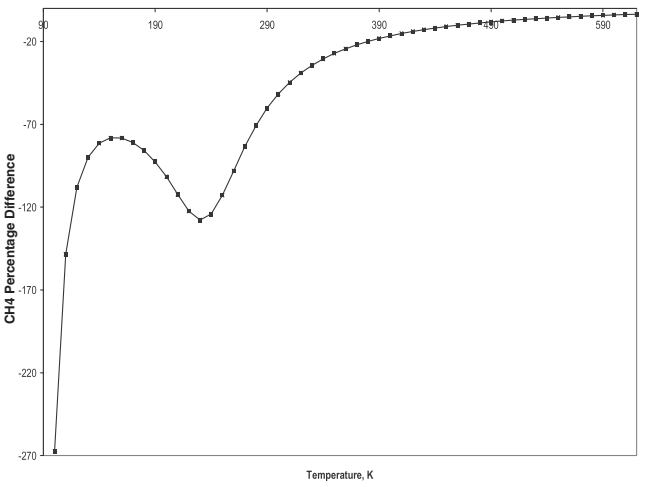

Fig. 14 CH_4, C_p % difference at 15 MPa.

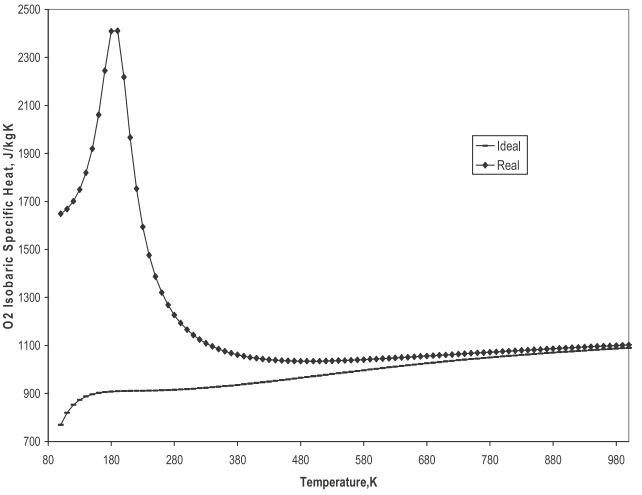

Fig. 15 O_2, C_p comparison at 15 MPa.

ideal-gas properties (ideal isobaric specific heat is lower than the corresponding real ones). This means that using ideal-gas properties CFD calculations will predict completely wrong gasdynamic fields. This is true at both low and high temperatures, as reported in Tables 2–4, where Z is close to one.

With this background, it is mandatory to find a complete and consistent description of the species properties, at conditions typical of LRE combustion. These properties have been calculated as described in the sections that follow, and are provided in polynomial form, to simplify implementation in CFD codes [13].

Equation of State and Isobaric Heat Capacity

National Institute of Standards and Technology (NIST) tables provide experimental data for density and isobaric heat capacity [14–20]. However, these data are available only for a range of temperature narrower than the one to be considered in combustion simulations. Thus, to describe density and heat capacity at temperatures different from the ones available from NIST, theories have been analyzed and compared [6,7] to find the one that provides the smallest departure at the highest temperature experimentally tested. This theory is the Lee–Kesler EOS [21] briefly reported next; it is a theory originally developed for the reference fluid *n-octane*.

Table 2 Temperature above which $(\Delta\rho/\rho) < 5\%$

	T, $(\Delta\rho/\rho) < 5\%$
CH_4	>380 K
CO_2	>550 K
H_2O	>1080 K
O_2	>310 K

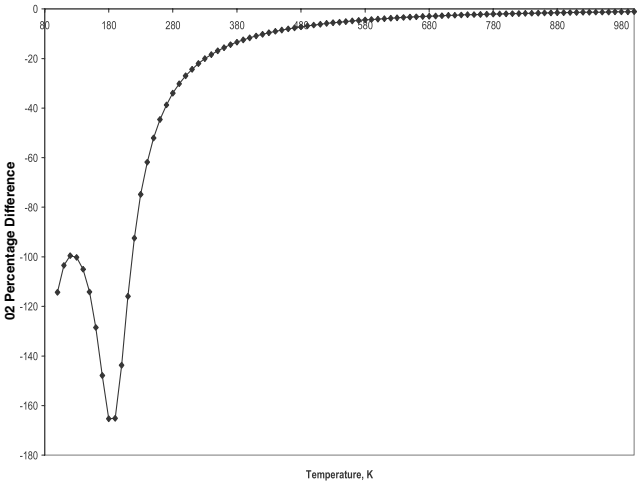

Fig. 16 O_2, C_p % difference at 15 MPa.

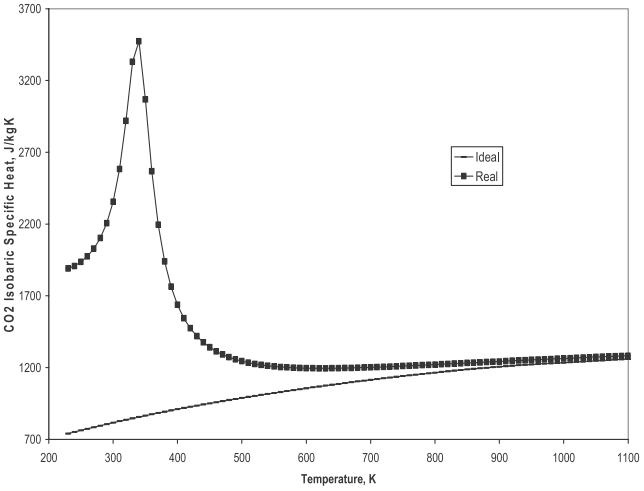

Fig. 19 CO_2, C_p comparison at 15 MPa.

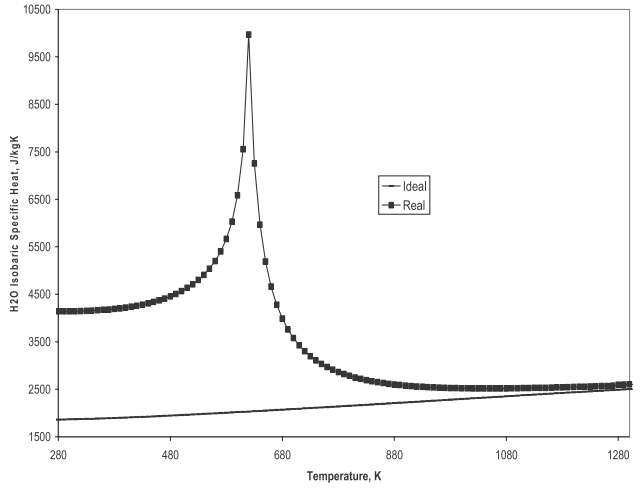

Fig. 17 H_2O, C_p comparison at 15 MPa.

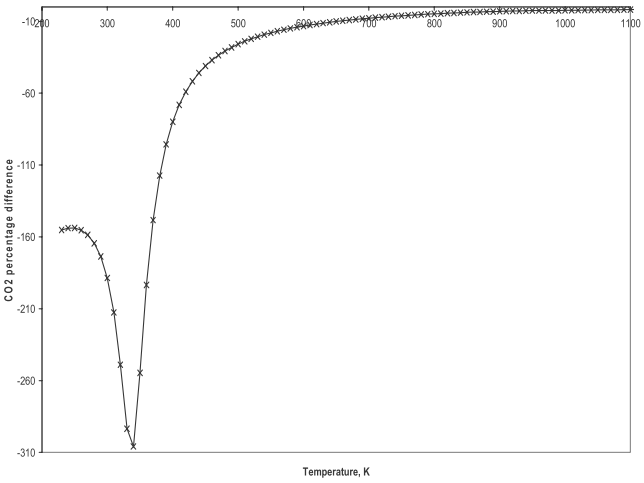

Fig. 20 CO_2, C_p % difference at 15 MPa.

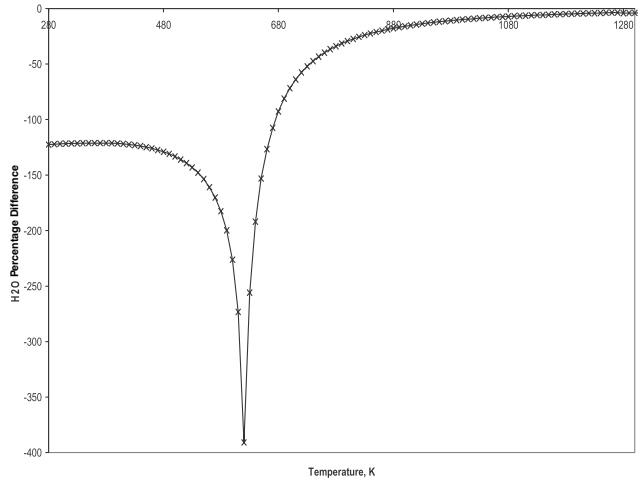

Fig. 18 H_2O, C_p % difference at 15 MPa.

Lee–Kesler Equation of State

The compressibility factor Z, as stated by the principle of corresponding states, can be correlated with the reduced temperature T_r ($T_r = T/T_c$) and pressure P_r ($P_r = P/P_c$) as

$$Z = f(P_r, T_r) \tag{2}$$

Equation (2) asserts that if pressure, volume, and temperature are normalized using the corresponding critical properties, the function relating reduced pressure to reduced volumes is the same for all substances; that is, the surface $P/P_c = f(V/V_c, T/T_c)$ is the same (for instance, an analytical expression embodying the principle of corresponding states is the van der Waals equation).

Rigorously speaking, however, this is not true for all substances but only for restricted sets, e.g., the set of heavy inert gases, Ar, Kr, Xe, or, with less accuracy, the set of isomers of hexane. For all other substances, the extension of this principle is an approximation with varying degrees of accuracy.

For hydrogen-bonded, polar molecules such as heavy hydrocarbons, or molecules with several degrees of freedom, this principle cannot be used, because their behavior cannot be described using an equation of state with only two parameters.

There are, however, extensions of the principle of corresponding states even for these substances, consisting in the introduction of a third parameter accounting for the "nonsphericity" of the molecule

Table 3 Temperature above which $(\Delta C_p/C_p) < 5\%$

	T, $(\Delta C_p/C_p) < 5\%$
CH_4	$380 < T < 1170$ K
CO_2	>800 K
H_2O	>1180 K
O_2	>560 K

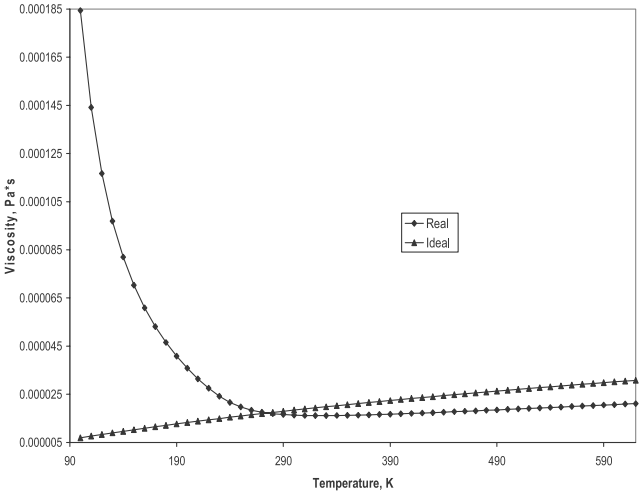

Fig. 21 CH_4, viscosity comparison at 15 MPa.

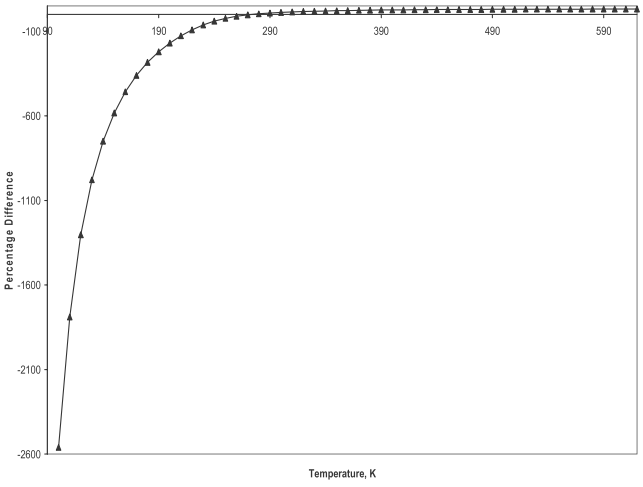

Fig. 22 CH_4, viscosity % difference at 15 MPa.

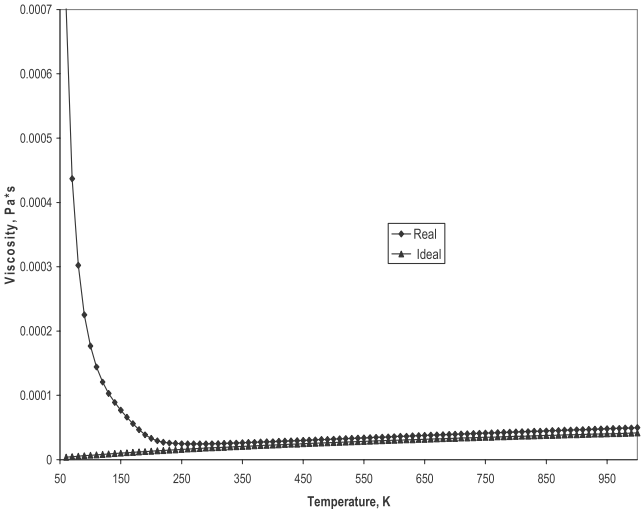

Fig. 23 O_2, viscosity comparison at 15 MPa.

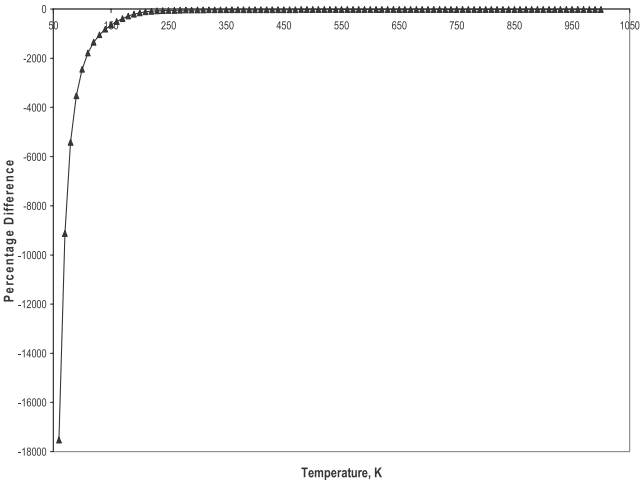

Fig. 24 O_2, viscosity % difference at 15 MPa.

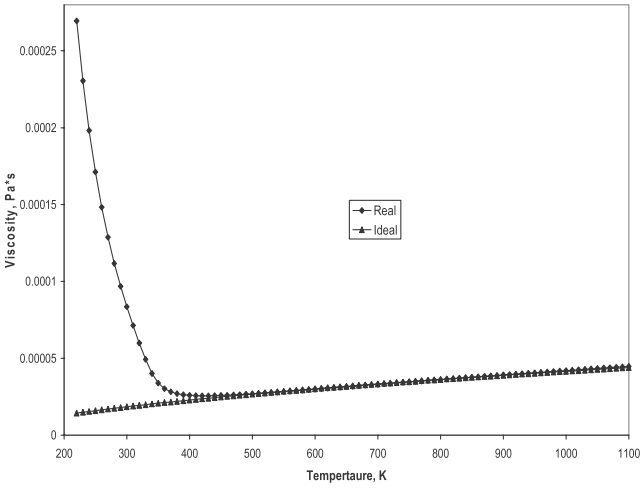

Fig. 25 CO_2, viscosity comparison at 15 MPa.

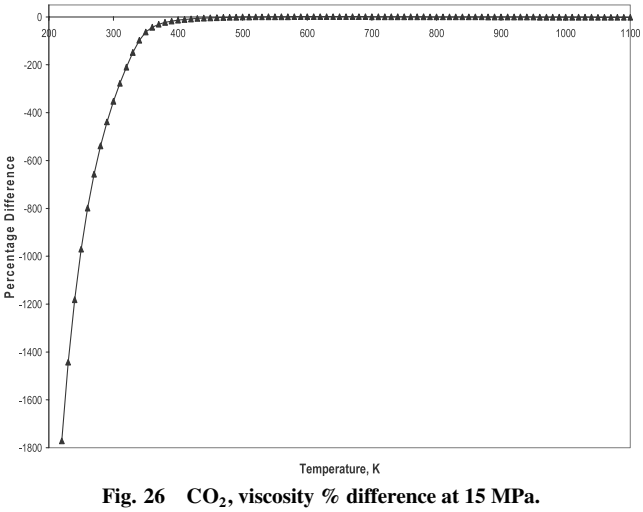

Fig. 26 CO_2, viscosity % difference at 15 MPa.

due, for instance, to noncentral electron distribution or to the large number of molecular degrees of freedom. The most widely used third parameter is the Pitzer's acentric factor ω.

Introducing this third parameter ω, substances with the same acentric factor have the same function $Z = f(T_r, P_r)$: the acentric factor univocally determines the critical compressibility factor that therefore may be different for different substances; this is the basis for the Lee–Kesler equation of state. Fluids with zero acentric factor are called simple fluids, whereas real fluids are those with an acentric factor greater than zero. However, instead of preparing several separate tables of Z, T_r, P_r for different ω, Z is approximated by using a linear expansion in the acentric factor:

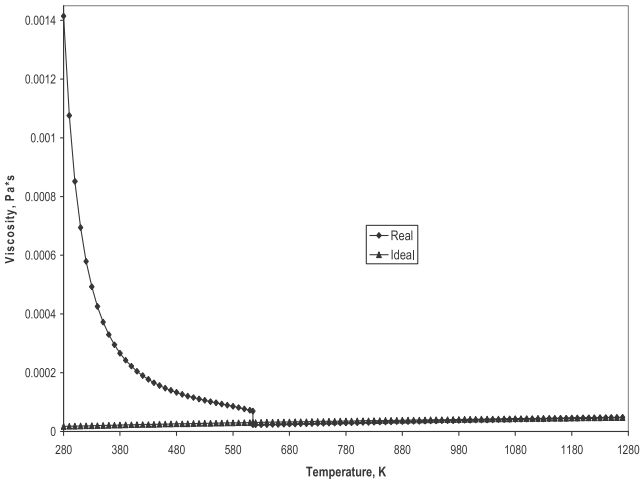

Fig. 27 H_2O, viscosity comparison at 15 MPa.

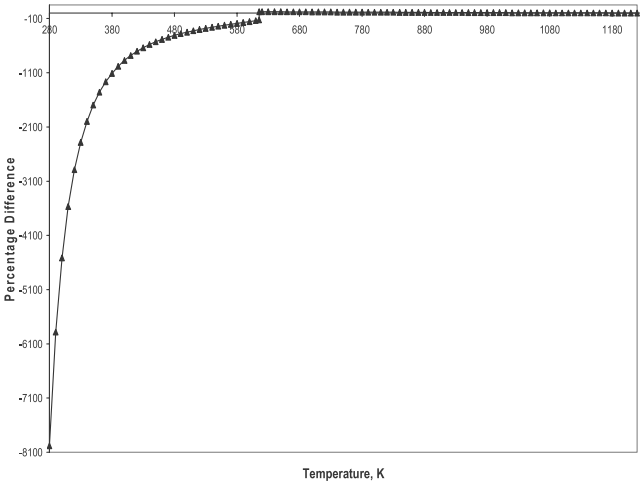

Fig. 28 H_2O, viscosity % difference at 15 MPa.

$$Z = Z^{(0)}(T_r, P_r) + \omega Z^{(1)}(T_r, P_r) \tag{3}$$

where $Z^{(0)}$ is the term for simple fluids (spherical symmetry), whereas $Z^{(1)}$ is the first-order deviation term accounting for molecule polarity.

To obtain this deviation term it is necessary to introduce a reference fluid, for which the Z surface has been determined as a function of known ω.

Table 4 Temperature above which $(\Delta\eta/\eta) < 5\%$

	T, $(\Delta\eta/\eta) < 5\%$
CH_4	$270 < T < 280$ K
CO_2	>450 K
H_2O	>1070 K
O_2	never (minimum 20%)

For historical reasons, the Lee–Kesler equation was developed with n-octane as the reference fluid, where $Z^{(0)}$ and $Z^{(1)}$ are the so-called Benedict–Webb–Rubin (BWR) equations, yielding pressure as a nonlinear function of temperature and density.

These equations are in widespread use because they easily fit specific substances and yield great accuracy in a broad range of temperatures and pressures. Unfortunately, the price for higher accuracy is the increased computational effort required in a CFD code: at a given temperature and pressure, density cannot be obtained directly ($Z^{(0)}$ and $Z^{(1)}$ are nonlinear functions) and many iterations are typically required.

The Lee–Kesler procedure is as follows: to determine Z of a species at a given temperature and pressure, first T_r and P_r and later the reduced ideal volume, defined as $V_r^{(0)} = P_C V^{(0)}/RT_C$, are calculated by the relationship

$$\frac{P_r V_r^{(0)}}{T_r} = 1 + \frac{B}{V_r^{(0)}} + \frac{C}{(V_r^{(0)})^2} + \frac{D}{(V_r^{(0)})^5} + \frac{c_4}{T_r^3 (V_r^{(0)})^2}\left[\beta + \frac{\gamma}{(V_r^{(0)})^2}\right] \cdot e^{\left[-\frac{\gamma}{(V_r^{(0)})^2}\right]} \tag{4}$$

where

$$B = b_1 - \frac{b_2}{T_r} - \frac{b_3}{T_r^2} - \frac{b_4}{T_r^3} \qquad C = c_1 - \frac{c_2}{T_r} + \frac{c_3}{T_r^3} \qquad D = d_1 + \frac{d_2}{T_r}$$

with b and c coefficients in Table 5.

Knowing $V_r^{(0)}$, the compressibility factor $Z^{(0)}$ for the simple fluid is determined from

$$Z^{(0)} = \frac{P_r V_r^{(0)}}{T_r} \tag{5}$$

With the same $T_r e P_r$, the $V_r^{(0)}$ is recalculated with *reference* fluid coefficients. The volume obtained is a reference reduced volume $V_r^{(R)}$ yielding a reference $Z^{(R)}$

$$Z^{(R)} = \frac{P_r V_r^{(R)}}{T_r} \tag{6}$$

The total fluid compressibility factor is then obtained as

$$Z = Z^{(0)} + \left(\frac{\omega}{\omega^{(R)}}\right)(Z^{(R)} - Z^{(0)}) \tag{7}$$

with the reference acentric factor $\omega^{(R)} = 0.39$ [6].

Note that at a given temperature and pressure, to determine the molar volume, Eq. (4) must be solved iteratively twice: once for the simple fluid and once for the reference fluid. Even when density and temperature are known, pressure cannot be obtained directly, and Eq. (4) must still be solved twice.

Once the EOS is defined, it is possible to calculate supercritical thermodynamic properties using so-called departure functions: they relate a thermodynamic property at some P, T to a reference state ($P = 0$ bar) at the same temperature, and may be calculated solely from PVT data or, equivalently, from an equation of state.

Analytical expressions for thermodynamic property (Helmholtz energy, entropy, enthalpy, and internal energy) are [22]:

$$A - A^0 = -\int_{\infty}^{V}\left(P - \frac{RT}{V}\right)\mathrm{d}V - RT\,\ell_n\frac{V}{V^o} \tag{8}$$

Table 5 Coefficients for Eq. (4)

	Simple fluid	Reference fluid		Simple fluid	Reference fluid		Simple fluid	Reference fluid		Simple fluid	Reference fluid
B_1	0.1181193	0.2026579	C_3	0.0	0.016901	b_4	0.030323	0.203488	$d_2 \times 10^4$	0.623689	0.0740336
B_2	0.265728	0.331511	C_4	0.042472	0.041577	c_1	0.0236744	0.0313385	β	0.65392	1.226
B_3	0.15479	0.027655	$d_1 \times 10^4$	0.155488	0.48736	c_2	0.0186984	0.0503618	γ	0.060167	0.03754

$$S - S^0 = -\frac{\partial}{\partial T}(A - A^0)_V = \int_\infty^V \left[\left(\frac{\partial P}{\partial T}\right)_V - \frac{R}{V}\right] \mathrm{d}V + R\,\ell n\,\frac{V}{V^o} \quad (9)$$

$$H - H^0 = (A - A^0) + T(S - S^0) + RT(Z - 1)$$
$$= \int_\infty^V \left[T\left(\frac{\partial P}{\partial T}\right)_V - P\right] \mathrm{d}V + RT(Z - 1) \quad (10)$$

$$U - U^0 = (A - A^0) + T(S - S^0) = \int_\infty^V \left[T\left(\frac{\partial P}{\partial T}\right)_V - P\right] \mathrm{d}V \quad (11)$$

Therefore, from any pressure-explicit equation of state and a definition of the reference state (P^0 or V^0), departure functions can be found. After calculating departure functions for heat capacities (at constant volume and constant pressure), the real-gas heat capacities will then be expressed as

$$c_v = c_v^0 + \Delta c_v \qquad c_p = c_p^0 + \Delta c_p \quad (12)$$

where the residual heat capacities Δc can be written as

$$\Delta c_v = T \int \left(\frac{\partial^2 P}{\partial T^2}\right)_V \mathrm{d}V \quad (13)$$

$$\Delta c_p = T \int \left(\frac{\partial^2 P}{\partial T^2}\right)_V \mathrm{d}V - \frac{T(\partial P/\partial T)_V^2}{(\partial P/\partial V)_T} - R \quad (14)$$

Equations (13) and (14) relate heat capacities in high-pressure, real-gas environments to those of an ideal gas.

Density and Isobaric Heat Capacity Results

Figures 29–36 report density and isobaric heat capacity predictions for O_2, CH_4, CO_2, and H_2O at typical LO_2-CH_4 liquid rocket engine chamber conditions: pressure 15 MPa and temperature from 100 to 6000 K (covering sub-, trans- and supercritical conditions).

As explained, predictions are obtained using the NIST data tables in their temperature range, and the data obtained with the Lee–Kesler EOS at lower and higher temperatures; polynomial fits of these predictions are at the end of this report.

The specific heat of every species past the critical temperature shows a peak: it indicates that the energy provided to the system is used not only to raise the temperature (constant during changes of state) but also to overcome the strong molecular attraction forces characteristic of the liquid state. Only after this occurs, the short range (weaker) forces among molecules become dominant and the fluid may be then defined a gas.

Transport Properties: Viscosity and Thermal Conductivity

Experimental data for viscosity and thermal conductivity are in NIST tables [13,23–30]. These data are available only in a range of temperature much narrower than that which is needed in combustion simulations. As for the case of thermodynamic properties, to predict viscosity and thermal conductivity at temperatures other than the ones available from NIST, theories have been analyzed and compared [6,7] to find the one that provides the smallest departure at the highest experimentally tested temperature. The best results have been obtained using the Chapman–Enskog theory with the Chung et al. method explained next [31–33].

Viscosity

The approach followed by Chung et al. [32] is based on the Chapman–Enskog theory [31]. This theory was originally formulated for dilute gases, but extension to high-pressure is possible. For high-pressure (real-gas) mixtures, the viscosity η is

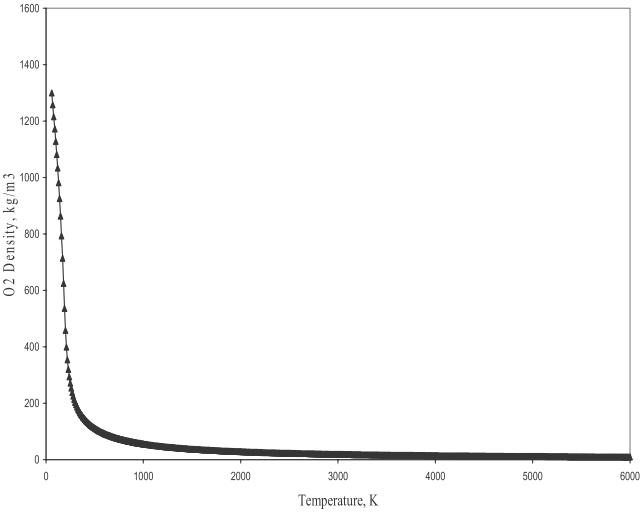

Fig. 29 O_2 density at 15 MPa.

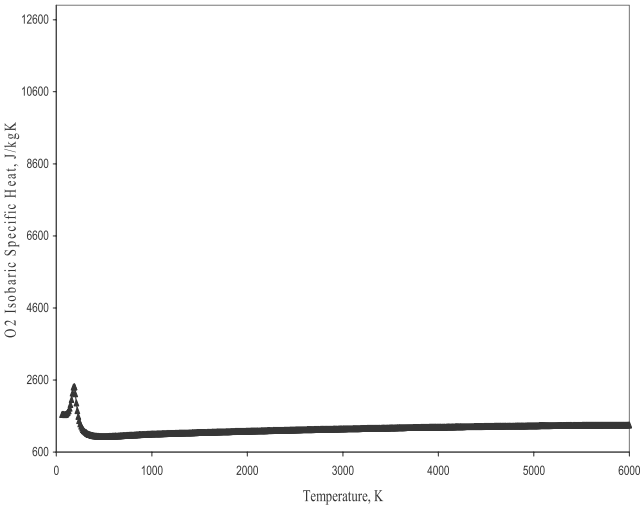

Fig. 30 O_2 isobaric specific heat at 15 MPa.

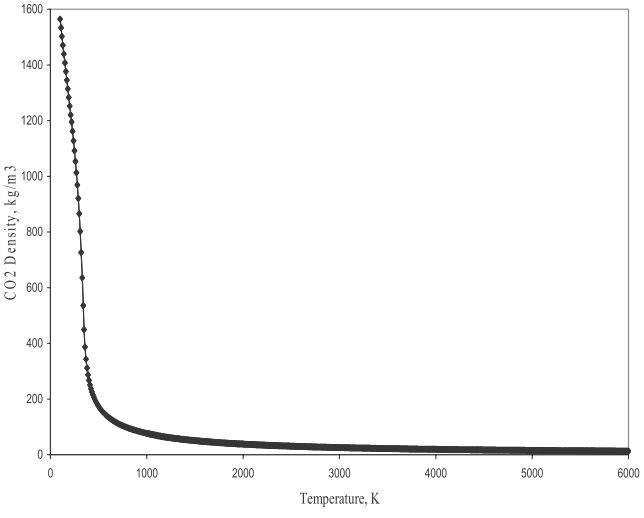

Fig. 31 CO_2 density at 15 MPa.

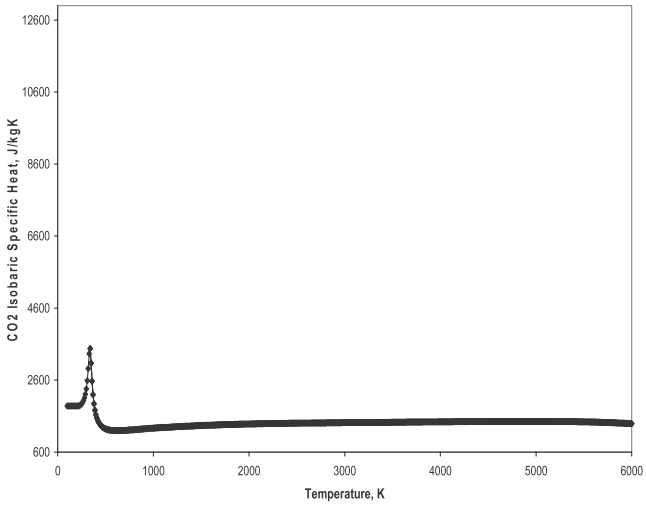

Fig. 32 CO_2 isobaric specific heat at 15 MPa.

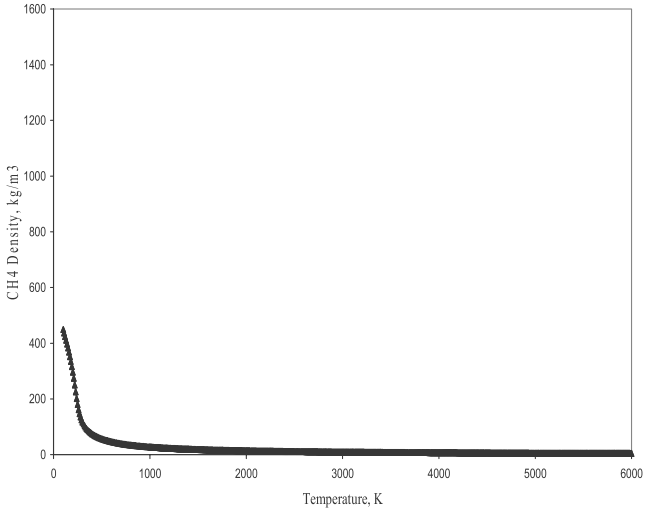

Fig. 33 CH_4 density at 15 MPa.

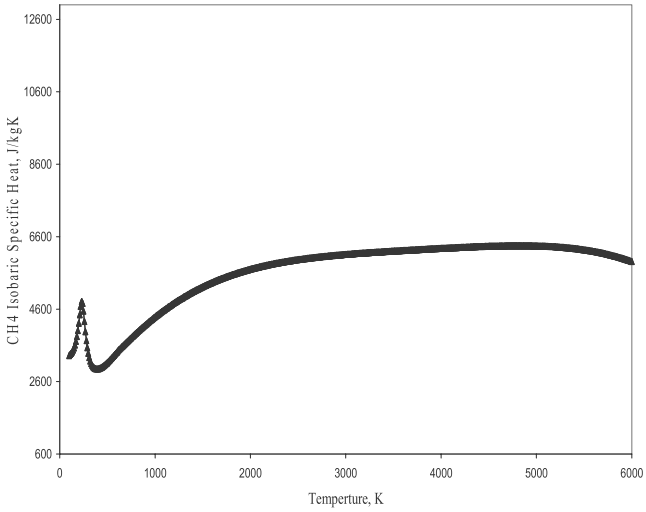

Fig. 34 CH_4 isobaric specific heat at 15 MPa.

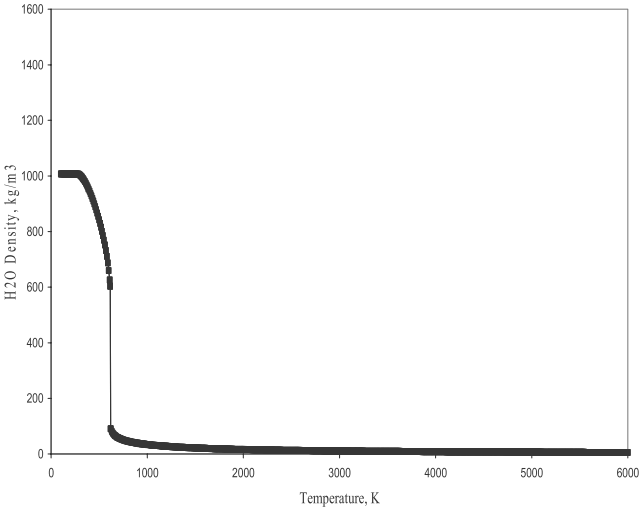

Fig. 35 H_2O density at 15 MPa.

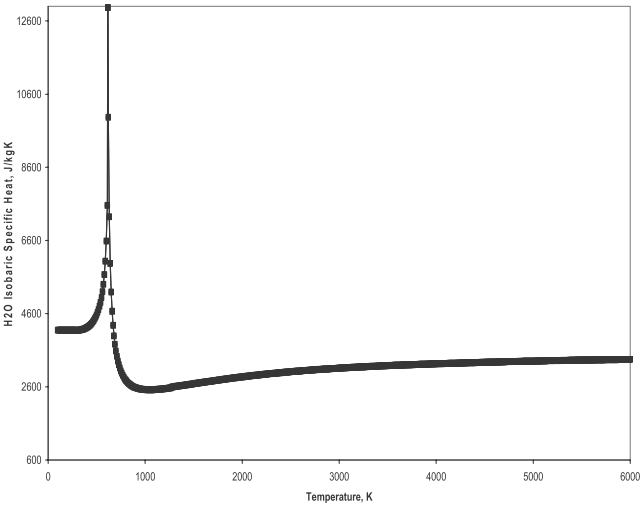

Fig. 36 H_2O isobaric specific heat at 15 MPa.

written

$$\eta = \eta * \eta^0 = \eta * \frac{40.785 F_{Cm} (M_m T)^{1/2}}{V_{Cm}^{2/3} \Omega_v} \tag{15}$$

where $\eta^0 =$ low pressure viscosity, μP ($1\ \mu\text{P} = 0.1\ \mu\text{Pa} \cdot \text{s}$); $\eta^* =$ correction term for high pressure viscosity; $M_m =$ mixture molecular weight, g/mol; $V_{C_m} =$ mixture critical volume, cm^3/mol; $\Omega_v =$ collision integral; $F_{C_m} = 1 - 0.2756\omega_m + 0.059035\mu_{\text{rm}}^4 + \kappa_m$.

In the equation for F_{C_m}, ω_m is the mixture acentric factor and κ_m is a special correction factor for highly polar substances such as alcohols and acids (see Table 6).

Table 6 Association factor κ

Compound	κ	Compound	κ
Methanol	0.215	n-pentanol	0.122
Ethanol	0.175	n-hexanol	0.114
n-propanol	0.143	n-heptanol	0.109
i-propanol	0.143	acetic acid	0.0916
n-butanol	0.132	water	0.076
i-butanol	0.132		

Table 7 Viscosity parameters in Chung et al.

$E_i = a_i + b_i\omega_m + c_i\mu_{r_m}^4 + d_i\kappa_m$									
i	a_i	b_i	c_i	d_i	i	a_i	b_i	c_i	d_i
1	6.324	50.412	−51.680	1189.0	6	−1.900	−12.537	4.985	−18.15
2	1.210×10^{-3}	-1.154×10^{-3}	-6.257×10^{-3}	0.03728	7	24.275	3.450	−11.291	69.35
3	5.283	254.209	−168.48	3989.0	8	0.7972	1.117	0.01235	−4.117
4	6.623	38.096	−8.464	31.42	9	−0.2382	0.06770	−0.8163	4.025
5	19.745	7.630	−14.354	31.53	10	0.06863	0.3479	0.5926	−0.727

The term μ_{r_m} is a dimensionless dipole moment which can be approximated by

$$\mu_{r_m} = 131.3\frac{\mu_m}{(V_{C_m}T_{C_m})^{1/2}} \tag{16}$$

where μ_m is expressed in debyes (1 D = 3.336×10^{-30} C × m).

The collision integral Ω_v is given the form

$$\Omega_v = [A(T^*)^{-B}] + C[\exp(-DT^*)] + E[\exp(-FT^*)] \tag{17}$$

where

$$T_m^* = 1.2593T_r \tag{18}$$

$A = 1.16145$, $B = 0.14874$, $C = 0.52487$, $D = 0.77320$, $E = 2.16178$, $F = 2.43787$.

The correction term η^* at high-pressure is expressed as

$$\eta^* = \left[\frac{1}{G_2} + E_6 y + \frac{\Omega_v}{F_{C_m}(T_m^*)^{1/2}}\eta^{**}\right] \tag{19}$$

where

$$y = \frac{\rho_m V_{C_m}}{6} \tag{20}$$

$$G_1 = \frac{1 - 0.5y}{(1-y)^3} \tag{21}$$

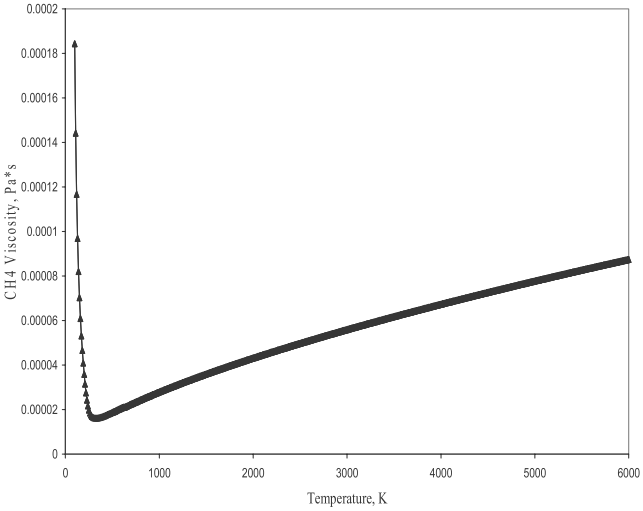

Fig. 37 CH_4 viscosity at 15 MPa.

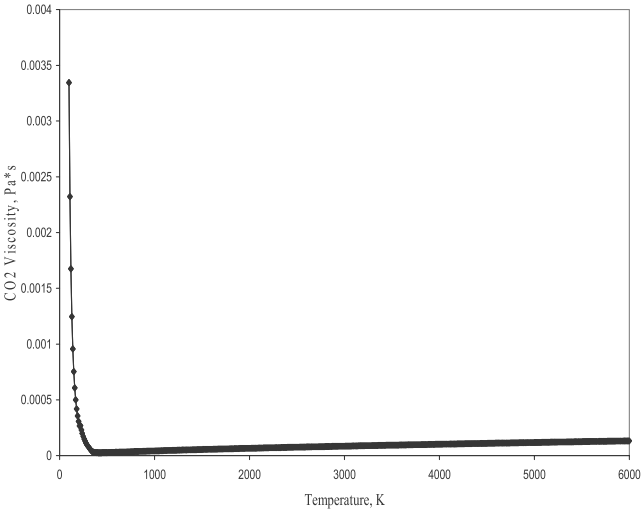

Fig. 39 CO_2 viscosity at 15 MPa.

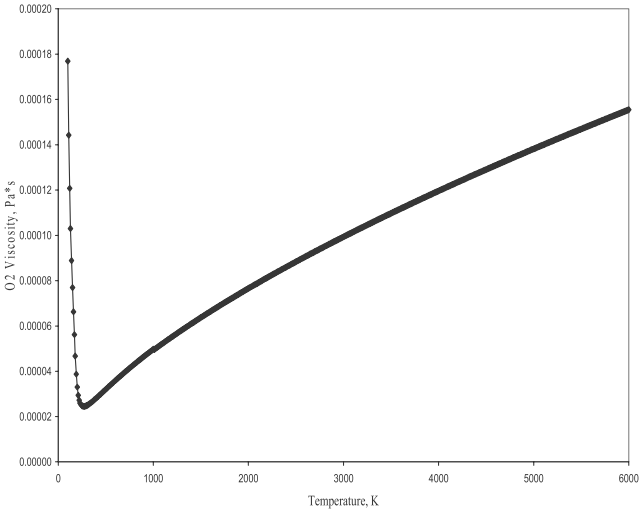

Fig. 38 O_2 viscosity at 15 MPa.

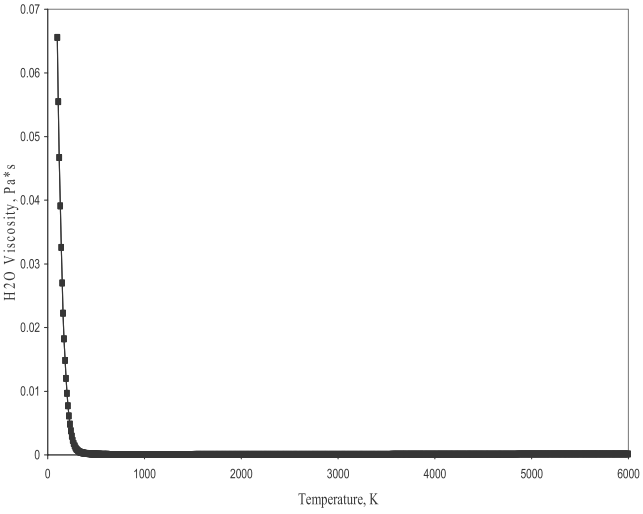

Fig. 40 H_2O viscosity at 15 MPa.

Table 8 B_i parameters for Chung et al. method [see Eqs. (24) and (25)]

$$B_i = a_i + b_i\omega_m + c_i\mu_{r_m}^4 + d_i\kappa_m$$

i	a_i	b_i	c_i	d_i
1	2.4166	0.74824	−0.91858	121.72
2	−0.50924	−1.5094	−49.991	69.983
3	6.6107	5.6207	64.760	27.039
4	14.543	−8.9139	−5.6379	74.344
5	0.79274	0.82019	−0.63969	6.3173
6	−5.8634	12.801	9.5893	65.529
7	91.089	12.811	−54.217	52.381

$$G_2 = \frac{E_1\{[1-\exp(-E_4 y)]/y\}}{E_1E_4 + E_2 + E_3} + \frac{E_2G_1\exp(E_5 y) + E_3G_1}{E_1E_4 + E_2 + E_3} \quad (22)$$

$$\eta^{**} = E_7y^2G_2\exp[E_8 + E_9(T_m^*)^{-1} + E_{10}(T_m^*)^{-2}] \quad (23)$$

Here, ρ_m is in mol/cm^3 and the parameters E_1–E_{10} are listed in Table 7 as linear functions of the mixture acentric factor ω_m, of the dimensionless dipole moment $\mu_{r_m}^4$ [Eq. (16)], and of the association factor κ_m.

In the limit of low-pressure and density, the y term vanishes, G_1 and G_2 approach unity, and η^{**} is negligible, so that $\eta \approx \eta^0$.

Viscosity Results

Figures 37–40 report viscosity predictions for O_2, CH_4, CO_2, and H_2O in the same T and P range used for thermodynamics properties; the polynomial fits of these predictions are reported at the end of this report. The viscosity drop across the critical point is evident.

Thermal Conductivity

For a high-pressure (real-gas) mixture, the approach in [33] results in a thermal conductivity λ given by

$$\lambda = \frac{31.2\eta^0\Psi}{M_m}(G_2^{*-1} + B_6y) + qB_7y^2T_r^{1/2}G_2^* \quad (24)$$

where M_m = mixture molecular weight, kg/mol; $\Psi = 1 + \alpha\{[0.215 + 0.28288\alpha - 1.061\beta + 0.26665Z]/[0.6366 + \beta Z + 1.061\alpha\beta]\}$; $\alpha = (C_{V_m}/\mathrm{R}) - 3/2$; $\beta = 0.7862 - 0.7109\omega + 1.1368\omega^2$; $N = 2.0 + 10.5T_r^2$; $q = 3.586 \times 10^{-3}(T_{C_m}/M_m)^{1/2}/V_{C_m}^{2/3}$.

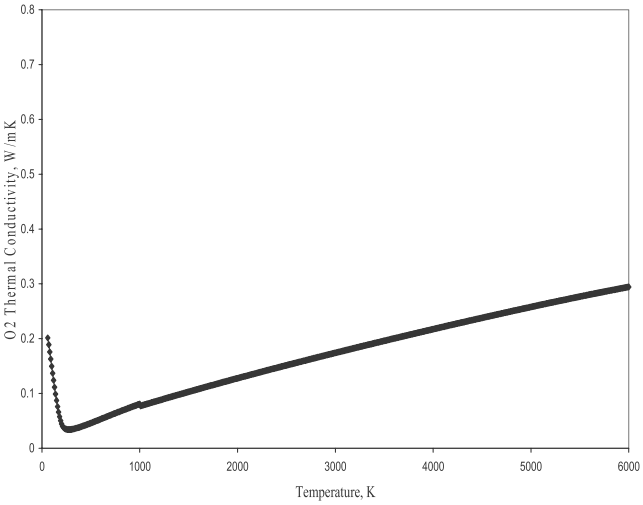

Fig. 42 O_2 thermal conductivity.

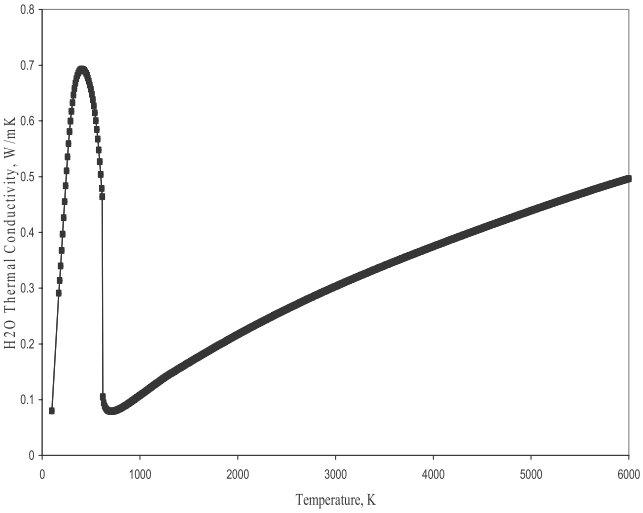

Fig. 43 H_2O thermal conductivity.

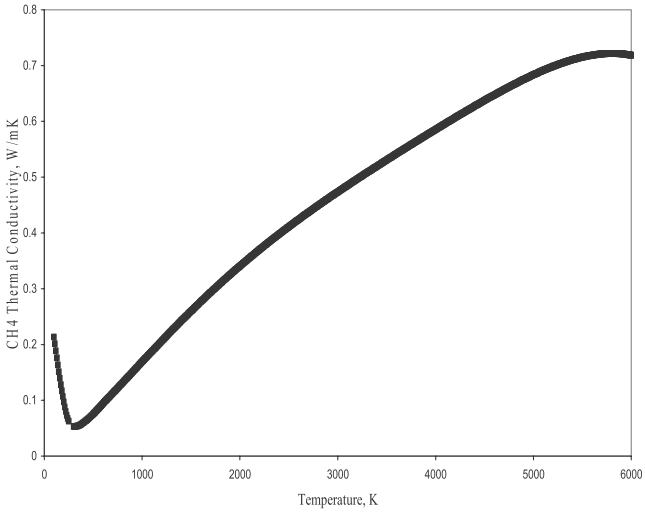

Fig. 41 CH_4 thermal conductivity.

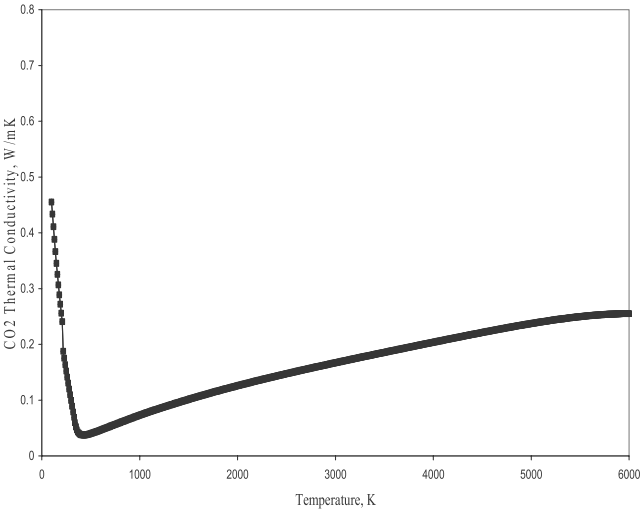

Fig. 44 CO_2 thermal conductivity.

The G_2^* parameter is to be calculated from

$$G_2^* = \frac{(B_1/y)[1-\exp(-B_4 y)]}{B_1 B_4 + B_2 + B_3} + \frac{B_2 G_1 \exp(B_5 y) + B_3 G_1}{B_1 B_4 + B_2 + B_3} \tag{25}$$

y and G_1 being the same used to calculate viscosity.

The parameter N is called the collision number, and represents the number of molecular collisions required to exchange a quantum of rotational energy with translational energy.

The B_i parameters are functions of the mixture acentric factor ω_m, of the reduced dipole moment μ_{r_m}, and of the association factor k_m (see Table 8).

Just as in the case of viscosity, if density is small, y approaches zero, G_1 and G_2 are essentially unity, and Eq. (24) returns the low-pressure thermal conductivity.

Thermal Conductivity Results

Figures 41–44 report the thermal conductivity predictions for O_2, CH_4, CO_2, and H_2O. Thermal conductivity is more difficult to model than viscosity, due to molecular internal degrees of freedom.

Polynomial Fits

Fitting polynomials of the properties predicted and shown in Figs. 29–44 are reported. These polynomials are of the sixth order, embrace a range of temperatures from 100 to 6000 K, at 15 MPa, and are divided into branches; the NIST table (experimental) data, Lee–Kesler EOS, or Chung et al. method data correspond to each branch.

CH_4

Density

if $100 < T < 300$ K, NIST table:
$y = -6.05381 \cdot 10^{-11}x^6 + 7.09839 \cdot 10^{-8}x^5 - 3.33287 \cdot 10^{-5}x^4 + 8.02451 \cdot 10^{-3}x^3 - 1.05013x^2 + 6.98147 \cdot 10^{1}x - 1.37217 \cdot 10^{3}$;
if $300 < T < 1000$ K, NIST table, and Lee–Kesler prediction:
$y = 8.79522 \cdot 10^{-5}x^6 - 3.76108 \cdot 10^{-11}x^5 + 6.62416 \cdot 10^{-8}x^4 - 6.16701 \cdot 10^{-5}x^3 + 3.22134 \cdot 10^{-2}x^2 - 9.1033x + 1.16182 \cdot 10^{3}$;
if $1000 < T < 6000$ K, Lee–Kesler prediction:
$y = 1.45376 \cdot 10^{-20}x^6 - 3.48106 \cdot 10^{-16}x^5 + 3.42293 \cdot 10^{-12}x^4 - 1.78227 \cdot 10^{-8}x^3 + 5.2785 \cdot 10^{-5}x^2 - 8.8528 \cdot 10^{-2}x + 7.79314 \cdot 10^{1}$.

Heat Capacity

if $100 < T < 230$ K, NIST table:
$y = -3.70622 \cdot 10^{-09}x^6 + 3.38455 \cdot 10^{-6}x^5 - 1.26917 \cdot 10^{-3}x^4 + 2.50775 \cdot 10^{-1}x^3 - 2.75251 \cdot 10^{1}x^2 + 1.5926 \cdot 10^{3}x - 3.46889 \cdot 10^{4}$;
if $230 < T < 500$ K, NIST table:
$y = -2.37008 \cdot 10^{-10}x^6 + 5.37781 \cdot 10^{-7}x^5 - 5.01852 \cdot 10^{-4}x^4 + 2.46095 \cdot 10^{-1}x^3 - 6.67021 \cdot 10^{1}x^2 + 9.43555 \cdot 10^{3}x - 5.37691 \cdot 10^{5}$;
if $500 < T < 6000$ K, NIST table, and Lee–Kesler prediction:
$y = 3.52416 \cdot 10^{-19}x^6 - 7.68272 \cdot 10^{-15}x^5 + 4.45259 \cdot 10^{-11}x^4 + 4.07532 \cdot 10^{-8}x^3 - 1.22403 \cdot 10^{-3}x^2 + 4.2784x + 1.28699 \cdot 10^{3}$.

Thermal Conductivity

if $100 < T < 250$ K, NIST table:
$y = -1.31383 \cdot 10^{-14}x^6 + 1.4796 \cdot 10^{-11}x^5 - 6.79702 \cdot 10^{-9}x^4 + 1.64451 \cdot 10^{-6}x^3 - 2.19991 \cdot 10^{-4}x^2 + 1.40814 \cdot 10^{-2}x - 9.43367 \cdot 10^{-2}$;
if $250 < T < 500$ K, NIST table:
$y = 3.96493 \cdot 10^{-16}x^6 - 1.00163 \cdot 10^{-12}x^5 + 1.05469 \cdot 10^{-9}x^4 - 5.93602 \cdot 10^{-7}x^3 + 1.88978 \cdot 10^{-4}x^2 - 3.22792 \cdot 10^{-2}x + 2.35797$;
if $500 < T < 6000$ K, NIST table, and Chung et al. prediction:
$y = 2.57832 \cdot 10^{-23}x^6 - 9.19839 \cdot 10^{-19}x^5 + 9.739 \cdot 10^{-15}x^4 - 4.36528 \cdot 10^{-11}x^3 + 7.40959 \cdot 10^{-8}x^2 + 1.35698 \cdot 10^{-4}x - 5.96054 \cdot 10^{-3}$.

Viscosity

if $100 < T < 250$ K, NIST table:
$y = 7.12524 \cdot 10^{-17}x^6 - 8.23341 \cdot 10^{-14}x^5 + 3.96366 \cdot 10^{-11}x^4 - 1.0202 \cdot 10^{-8}x^3 + 1.48825 \cdot 10^{-6}x^2 - 1.18021 \cdot 10^{-4}x - 4.09432 \cdot 10^{-3}$;
if $250 < T < 500$ K, NIST table:
$y = 3.36019 \cdot 10^{-19}x^6 - 8.11111 \cdot 10^{-16}x^5 + 8.12808 \cdot 10^{-13}x^4 - 4.33168 \cdot 10^{-10}x^3 + 1.29648 \cdot 10^{-7}x^2 - 2.06832 \cdot 10^{-5}x + 1.39082 \cdot 10^{-3}$;
if $500 < T < 6000$ K, NIST table, and Chung et al. prediction:
$y = -3.28136 \cdot 10^{-29}x^6 + 4.87301 \cdot 10^{-24}x^5 - 9.69787 \cdot 10^{-20}x^4 + 8.51181 \cdot 10^{-16}x^3 - 4.36703 \cdot 10^{-12}x^2 + 2.37311 \cdot 10^{-8}x + 7.79291 \cdot 10^{-6}$.

O_2

Density

if $60 < T < 300$ K, NIST table:
$y = 9.51162 \cdot 10^{-13}x^6 - 1.75012 \cdot 10^{-8}x^5 + 1.50615 \cdot 10^{-5}x^4 - 4.83018 \cdot 10^{-3}x^3 + 6.98075 \cdot 10^{-1}x^2 - 5.01477 \cdot 10^{1}x + 2.6641 \cdot 10^{3}$;
if $300 < T < 1000$ K, NIST table:
$y = 7.3875 \cdot 10^{-15}x^6 - 3.20547 \cdot 10^{-11}x^5 + 5.75511 \cdot 10^{-8}x^4 - 5.50028 \cdot 10^{-5}x^3 + 2.98409 \cdot 10^{-2}x^2 - 8.96431x + 1.29811 \cdot 10^{3}$;
if $1000 < T < 6000$ K, NIST table, and Lee–Kesler prediction:
$y = 2.87683 \cdot 10^{-20}x^6 - 6.8952 \cdot 10^{-16}x^5 + 6.78846 \cdot 10^{-12}x^4 - 3.54044 \cdot 10^{-8}x^3 + 1.05089 \cdot 10^{-4}x^2 - 1.76772 \cdot 10^{-1}x + 1.56126 \cdot 10^{2}$.

Heat Capacity

if $60 < T < 190$ K, NIST table:
$y = -7.52358 \cdot 10^{-9}x^6 + 5.27508 \cdot 10^{-6}x^5 - 1.50339 \cdot 10^{-3}x^4 + 2.23289 \cdot 10^{-1}x^3 - 1.81883 \cdot 10^{1}x^2 + 7.68284 \cdot 10^{2}x - 1.14738 \cdot 10^{4}$;

if $190 < T < 620$ K, NIST table:
$y = 4.11956 \cdot 10^{-12}x^6 - 1.14522 \cdot 10^{-8}x^5 + 1.31289 \cdot 10^{-5}x^4 - 7.95068 \cdot 10^{-3}x^3 + 2.68734x^2 - 4.82289 \cdot 10^2 x + 3.71347 \cdot 10^4$;
if $620 < T < 6000$ K, NIST table, and Lee–Kesler prediction:
$y = -1.03229 \cdot 10^{-19}x^6 + 2.19459 \cdot 10^{-15}x^5 - 1.87693 \cdot 10^{-11}x^4 + 8.24765 \cdot 10^{-8}x^3 - 2.02669 \cdot 10^{-4}x^2 + 3.34663 \cdot 10^{-1}x + 9.01747 \cdot 10^2$.

Thermal Conductivity

if $60 < T < 300$ K, NIST table:
$y = 8.67304 \cdot 10^{-15}x^6 - 9.73184 \cdot 10^{-12}x^5 + 4.21229 \cdot 10^{-9}x^4 - 8.80612 \cdot 10^{-7}x^3 + 9.48322 \cdot 10^{-5}x^2 - 6.3376 \cdot 10^{-3}x + 3.8361 \cdot 10^{-1}$;
if $300 < T < 6000$ K, NIST table, and Chung et al. prediction:
$y = -2.80237 \cdot 10^{-23}x^6 + 5.7916 \cdot 10^{-19}x^5 - 4.76621 \cdot 10^{-15}x^4 + 1.98637 \cdot 10^{-11}x^3 - 4.54252 \cdot 10^{-8}x^2 + 1.02437 \cdot 10^{-4}x + 5.11095 \cdot 10^{-3}$.

Viscosity

if $60 < T < 300$ K, NIST table:
$y = 1.59891 \cdot 10^{-16}x^6 - 1.9089 \cdot 10^{-13}x^5 + 9.24691 \cdot 10^{-11}x^4 - 2.32356 \cdot 10^{-8}x^3 + 3.19845 \cdot 10^{-6}x^2 - 2.30432 \cdot 10^{-4}x + 6.96395 \cdot 10^{-3}$;
if $300 < T < 6000$ K, NIST table, and Chung et al. prediction:
$y = -5.25679 \cdot 10^{-27}x^6 + 1.16891 \cdot 10^{-22}x^5 - 1.06184 \cdot 10^{-18}x^4 + 5.16672 \cdot 10^{-15}x^3 - 1.5576 \cdot 10^{-11}x^2 + 5.03677 \cdot 10^{-8}x + 1.03527 \cdot 10^{-5}$.

H_2O

Density

if $100 < T < 615.31$ K, NIST table:
$y = -3.50794 \cdot 10^{-13}x^6 + 6.71534 \cdot 10^{-10}x^5 - 4.97616 \cdot 10^{-7}x^4 + 1.76667 \cdot 10^{-4}x^3 - 3.17852 \cdot 10^{-2}x^2 + 2.77444x + 9.14204 \cdot 10^2$;
if $615.31 < T < 620$ K, NIST table: $y = -1.09415 \cdot 10^2 x + 6.79278 \cdot 10^4$;
if $620 < T < 6000$ K, NIST table, and Lee–Kesler prediction:
$y = 1.66769 \cdot 10^{-19}x^6 - 3.62201 \cdot 10^{-15}x^5 + 3.14876 \cdot 10^{-11}x^4 - 1.39747 \cdot 10^{-7}x^3 + 3.33933 \cdot 10^{-4}x^2 - 4.13174 \cdot 10^{-1}x + 2.2618 \cdot 10^2$.

Heat Capacity

if $100 < T < 615.31$ K, NIST table:
$y = 4.35642 \cdot 10^{-11}x^6 - 8.69603 \cdot 10^{-8}x^5 + 6.8848 \cdot 10^{-5}x^4 - 2.74488 \cdot 10^{-2}x^3 + 5.76537x^2 - 6.0024 \cdot 10^2 x + 2.82001 \cdot 10^4$;
if $615.31 < T < 800$ K, NIST table:
$y = 1.25906 \cdot 10^{-8}x^6 - 5.43961 \cdot 10^{-5}x^5 + 9.78046 \cdot 10^{-2}x^4 - 9.36777 \cdot 10^1 x^3 + 5.04112 \cdot 10^4 x^2 - 1.44516 \cdot 10^7 x + 1.72429 \cdot 10^9$;
if $800 < T < 6000$ K, NIST table, and Lee–Kesler prediction:
$y = 2.56171 \cdot 10^{-18}x^6 - 5.66853 \cdot 10^{-14}x^5 + 5.00439 \cdot 10^{-10}x^4 - 2.23121 \cdot 10^{-6}x^3 + 5.18087 \cdot 10^{-3}x^2 - 5.53503x + 4.70415 \cdot 10^3$.

Thermal Conductivity

if $100 < T < 620$ K, NIST table:
$y = -2.56155 \cdot 10^{-15}x^6 + 5.17764 \cdot 10^{-12}x^5 - 4.10916 \cdot 10^{-9}x^4 + 1.61983 \cdot 10^{-6}x^3 - 3.35836 \cdot 10^{-4}x^2 + 3.75005 \cdot 10^{-2}x - 1.57256$;
if $615.31 < T < 1000$ K, NIST table:
$y = 5.62597 \cdot 10^{-16}x^6 - 2.82222 \cdot 10^{-12}x^5 + 5.87865 \cdot 10^{-9}x^4 - 6.50889 \cdot 10^{-61}x^3 + 4.04083 \cdot 10^{-3}x^2 - 1.33387x + 1.83003 \cdot 10^2$;
if $1000 < T < 6000$ K, NIST table, and Chung et al. prediction:
$y = -3.06909 \cdot 10^{-23}x^6 + 6.25402 \cdot 10^{-19}x^5 - 5.17275 \cdot 10^{-15}x^4 + 2.31922 \cdot 10^{-11}x^3 - 6.81027 \cdot 10^{-8}x^2 - 2.10675x - 5.29262 \cdot 10^{-2}$.

Viscosity

if $100 < T < 615.31$, NIST table:
$y = 2.66244 \cdot 10^{-17}x^6 - 7.60818 \cdot 10^{-14}x^5 + 8.99203 \cdot 10^{-11}x^4 - 5.62854 \cdot 10^{-8}x^3 + 1.96945 \cdot 10^{-5}x^2 - 3.65741 \cdot 10^{-3}x + 2.82407 \cdot 10^{-1}$;
if $615.31 < T < 620$ K, NIST table: $y = -9.94478 \cdot 10^{-6}x + 6.18862 \cdot 10^{-3}$;
if $620 < T < 6000$ K, NIST table, and Chung et al. prediction:
$y = -1.34938 \cdot 10^{-26}x^6 + 3.12722 \cdot 10^{-22}x^5 - 2.95515 \cdot 10^{-18}x^4 + 1.4715 \cdot 10^{-14}x^3 - 4.22273 \cdot 10^{-11}x^2 + 8.78545 \cdot 10^{-8}x - 1.90839 \cdot 10^{-5}$.

CO_2

Density

if $100 < T < 450$ K, Lee–Kesler prediction, and NIST table:
$y = -3.20861 \cdot 10^{-11}x^6 + 5.29453 \cdot 10^{-8}x^5 - 3.44612 \cdot 10^{-5}x^4 + 1.12649 \cdot 10^{-2}x^3 - 1.94835x^2 + 1.65981 \cdot 10^2 x - 3.88396 \cdot 10^3$;
if $450 < T < 1000$ K, NIST table:
$y = 1.61993 \cdot 10^{-14}x^6 - 7.65617 \cdot 10^{-11}x^5 + 1.50445 \cdot 10^{-7}x^4 - 1.5775 \cdot 10^{-4}x^3 + 9.35717 \cdot 10^{-2}x^2 - 3.01262 \cdot 10^1 x + 4.29942 \cdot 10^3$;
if $620 < T < 6000$ K, NIST table, and Lee–Kesler prediction:
$y = 5.09372 \cdot 10^{-20}x^6 - 1.20371 \cdot 10^{-15}x^5 + 1.16407 \cdot 10^{-11}x^4 - 5.93234 \cdot 10^{-8}x^3 + 1.70766 \cdot 10^{-4}x^2 - 2.75471 \cdot 10^{-1}x + 2.29563 \cdot 10^2$.

Heat Capacity

if $100 < T < 340$ K, NIST table:
$y = -2.95183 \cdot 10^{-10}x^6 + 3.83784 \cdot 10^{-7}x^5 - 1.99475 \cdot 10^{-4}x^4 + 5.32225 \cdot 10^{-2}x^3 - 7.69618x^2 + 5.71952 \cdot 10^2 x - 1.51864 \cdot 10^4$;
if $340 < T < 600$ K, NIST table:
$y = -3.3929 \cdot 10^{-11}x^6 + 8.24304 \cdot 10^{-8}x^5 - 7.73901 \cdot 10^{-5}x^4 + 3.36556 \cdot 10^{-2}x^3 - 5.62267x^2 - 3.23351 \cdot 10^2 x + 1.52718 \cdot 10^5$;
if $600 < T < 6000$ K, NIST table, and Lee–Kesler prediction:
$y = 1.11715 \cdot 10^{-19}x^6 - 2.48631 \cdot 10^{-15}x^5 + 1.91709 \cdot 10^{-11}x^4 - 5.82412 \cdot 10^{-8}x^3 + 2.05127 \cdot 10^{-5}x^2 + 2.44805 \cdot 10^{-1}x + 1.03923 \cdot 10^3$.

Thermal Conductivity

if $1000 < T < 340$ K, Chung et al. prediction, and NIST table:
$y = 2.18527 \cdot 10^{-14}x^6 - 3.15089 \cdot 10^{-11}x^5 + 1.82371 \cdot 10^{-8}x^4 - 5.39351 \cdot 10^{-6}x^3 + 8.58262 \cdot 10^{-4}x^2 - 7.17165 \cdot 10^{-2}x + 2.91068$;

if $350 < T < 700$ K, NIST table:
$y = 3.99779 \cdot 10^{-16}x^6 - 1.33104 \cdot 10^{-12}x^5 + 1.83631 \cdot 10^{-9}x^4 - 1.34405 \cdot 10^{-6}x^3 + 5.5071 \cdot 10^{-4}x^2 - 1.19786 \cdot 10^{-1}x + 1.08408 \cdot 10^{1}$;
if $700 < T < 6000$ K, NIST table, and Chung et al. prediction:
$y = -5.83303 \cdot 10^{-24}x^6 + 6.42621 \cdot 10^{-20}x^5 - 4.16035 \cdot 10^{-16}x^4 + 3.27186 \cdot 10^{-12}x^3 - 1.91731 \cdot 10^{-8}x^2 + 9.22219 \cdot 10^{-5}x - 3.11668 \cdot 10^{-3}$.

Viscosity

if $100 < T < 350$ K, Chung et al. prediction, and NIST table:
$y = 3.02663 \cdot 10^{-16}x^6 - 4.55023 \cdot 10^{-13}x^5 + 2.81678 \cdot 10^{-10}x^4 - 9.20033 \cdot 10^{-8}x^3 + 1.67621 \cdot 10^{-5}x^2 - 1.62361 \cdot 10^{-3}x + 6.61431 \cdot 10^{-2}$;
if $350 < T < 600$ K, NIST table:
$y = 1.46842 \cdot 10^{-18}x^6 - 4.37038 \cdot 10^{-15}x^5 + 5.39936 \cdot 10^{-12}x^4 - 3.54486 \cdot 10^{-9}x^3 + 1.30473 \cdot 10^{-6}x^2 - 2.55327 \cdot 10^{-4}x + 2.0785 \cdot 10^{-2}$;
if $600 < T < 6000$ K, NIST table, and Chung et al. prediction:
$y = -4.58155 \cdot 10^{-27}x^6 + 1.08654 \cdot 10^{-22}x^5 - 1.05925 \cdot 10^{-18}x^4 + 5.51989 \cdot 10^{-15}x^3 - 1.72375 \cdot 10^{-11}x^2 + 4.94878 \cdot 10^{-8}x + 5.2131 \cdot 10^{-6}$.

Conclusions

The intention to use CH_4 and LO_2 as liquid propellants in future launch vehicles has suggested study of the thermophysical properties of these species, and of their products, at typical LRE combustion chamber conditions.

Preliminary analysis of the compressibility factor Z for CH_4, O_2, H_2O, and CO_2 (the main species in combustion of these propellants) has shown that differences of thermophysical properties between ideal and real gases are large or very large. In fact, this analysis has shown that the differences are so high that to neglect real-gas behavior could lead to significantly erroneous thermofluidynamic fields (results of CFD simulations comparisons using ideal and real-gas assumptions are reported in [7]). Thus, a complete and consistent description of the gas properties behavior, at least for these species, has been performed, and thermophysical properties have been modeled.

Accordingly, this report provides sixth-order fitting polynomials that describe the thermophysical properties of $CH_4/O_2/CO_2$ and H_2O at 15 MPa and in the temperature range of 100–6000 K.

These polynomials have been defined by using both experimental data (NIST tables) when available, and the Lee–Kesler theory (for thermodynamic properties), and the Chung et al. theory and method (for transport properties) in the temperature range not covered by existing data. Among these properties, the thermal conductivity has been the most difficult to define, due to the difficulty of modeling the internal degrees of freedom.

References

[1] Kalmykov, G. P., and Mossolov, S. V., "Liquid Rocket Engines Working on Oxygen+Methane for Space Transportation Systems of the XXI Century (on the Results of Scientific and Experimental Studies)," *51th International Astronautical Congress*, International Astronautical Congress Paper 00-S.2.10, Oct. 2000.

[2] Burkardt, H., Sippel, M., Herbertz, A., and Klevansky, J., "Effects of the Choice Between Kerosene and Methane on Size and Performance of Reusable Liquid Booster Stages," *39th Joint Propulsion Conference and Exhibit*, AIAA Paper 2003-3122, July 2003.

[3] Pempie, P., Frohlich, T., and Vernin, H., "Lox-Methane and Lox-Kerosene High Thrust Engine Trade-Off," *37th Joint Propulsion Conference and Exhibit*, AIAA Paper 2001-3542, July 2001.

[4] Klepikov, I. A., Katorgin, B. I., and Chvanov, V. K., "The New Generation of Rocket Engines, Operating by Ecologically Safe Propellant 'Liquid Oxygen and Liquefied Natural Gas (Methane)'," *48th International Astronautical Congress*, International Astronautical Congress Paper 97-S.1.03, 1997.

[5] Gotz, A., Mading, C., Brummer, L., and Haesker, D., "Application of Non-Toxic Propellants for Future Advanced Launch Vehicles," *37th Joint Propulsion Conference*, AIAA Paper 2001-3546, July 2001.

[6] Congiunti, A., Bruno, C., and Giacomazzi, E., "Supercritical Combustion Properties," *41st Aerospace Science Meeting and Exhibition*, AIAA Paper 2003-478, Jan. 2003.

[7] Minotti, A., "Sub-Trans and Supercritical Combustion Modelling for LOx-HC Propulsion," Ph.D. Thesis, Univ. of Rome "La Sapienza", Dept. of Mechanical and Aeronautical Engineering, 2007.

[8] Gordon, S., McBride, B. J., and Zeleznik, F. J., "Computer Program for Calculation of Complex Chemical Equilibrium Composition and Applications, Supplement I-Transport Properties," NASA TM-86885, 1984.

[9] Gordon, S., and McBride, B. J., "Computer Program for Calculating and Fitting Thermodynamic Functions," NASA RP-1271, 1992.

[10] Gordon, S., McBride, B. J., and Reno, M. A., "Thermodynamic Data for Fifty Reference Elements," NASA TP-3287, 1993.

[11] Gordon, S., McBride, B. J., and Reno, M. A., "Coefficients for Calculating Thermodynamic and Transport Properties of Individual Species," NASA TM-4513, 1993.

[12] Fluent Software Package Handbook, Ver. 6.2.16, Fluent, Lebanon, NH, 2005, Chap. 8.4.2.

[13] Vesovic, V., Wakeham, W. A., Olchowy, G. A., Sengers, J. V., Watson, J. T. R., and Millat, J., "The Transport Properties of Carbon Dioxide," *Journal of Physical and Chemical Reference Data*, Vol. 19, No. 3, May 1990, pp. 763–808.

[14] Setzmann, U., and Wagner, W., "A New Method for Optimizing the Structure of Thermodynamic Correlation Equations," *International Journal of Thermophysics*, Vol. 10, No. 6, Nov. 1989, pp. 1103–1126.

[15] Saul, A., and Wagner, W., "A Fundamental Equation for Water Covering the Range from Melting Line to 1273 K at Pressure up to 25000 MPa," *Journal of Physical and Chemical Reference Data*, Vol. 18, No. 4, 1989, pp. 1537–1564.

[16] McDowell, R. A., and Kruse, F. H., "Thermodynamic Functions of Methane," *Journal of Chemical and Engineering Data*, Vol. 7, No. 1, 1963, pp. 547–548.

[17] Friend, D. G., Ely, J. F., and Ingham, H., "Thermophysical Properties of Methane," *Journal of Physical and Chemical Reference Data*, Vol. 18, No. 2, 1989, pp. 583–638.

[18] Scmidth, R., and Wagner, W., "New Form of the Equation of State for Pure Substances and Its Application to Oxygen," *Fluid Phase Equilibria*, Vol. 19, No. 3, 1985, pp. 175–200.

[19] Wagner, W., and Pruss, A., "IAPWS Formulation 1995 for the Thermodynamic Properties of Ordinary Water Substance for General and Scientific Use," *Journal of Physical and Chemical Reference Data*, Vol. 31, No. 2, 2002, pp. 387–535.

[20] Span, R., and Wagner, W., "New Equation of State for Carbon Dioxide Covering the Fluid Region from the Triple Point Temperature to 1100 K at Pressure up to 800 MPa," *Journal of Physical and Chemical Reference Data*, Vol. 25, No. 6, 1986, pp. 1509–1596.

[21] Lee, B. I., and Kesler, M. G., "A Generalized Thermodynamic Correlation Based on Three-Parameter Corresponding States," *AIChE Journal*, Vol. 21, No. 3, 1975, pp. 510–527.

[22] Reid, R. C., Prausnitz, J. M., and Poling, B. E., "*The Properties of Gases and Liquids*," McGraw–Hill International Editions, 4th ed., McGraw–Hill, Singapore, 1989, Chaps. 1–5, 8–11.

[23] Sengers, J. V., and Basu, J. V., "Representative Equations for the Thermodynamic and Transport Properties of Fluids near the Gas-Liquid Critical Point," NASA CR 3424, May 1981.

[24] Hanley, H. J. M., and Klein, M., National Inst. of Standards and Technology, TN 628, 1972.

[25] Klein, M., Hanley, H. J. M., Smith, F. J., and Holland, P., Tables of Collision Integrals and Second Virial Coefficients for the (m,6,8) Intermolecular Potential Function, *Nation Bureau of Standards (U.S.) Monograph*, Vol. 47, No. 1, 1974.

[26] Setzmann, U., and Wagner, W., "New Equation of State and Tables of Thermodynamic Properties for Methane Covering the Range from the Melting Line to 625 K at Pressure up to 1000 MPa," *Journal of Physical and Chemical Reference Data*, Vol. 20, No. 6, 1991, pp. 1061–1151.

[27] Friend, D. G., Ely, J. F., and Ingham, J. F., National Institute of Standard and Technology, TN 1325, 1989.

[28] Vicentini-Missoni, M., Levelt Sengers, J. M. H., and Green, M. S., Scaling Analysis of Thermodynamic Properties in Critical Region of Fluids, *Journal of Research of the National Bureau of Standards, Section A: Physics and Chemistry*, Vol. 73, 1969, p. 563;*Physical Review Letters*, Vol. 22, 1969, pp. 389–393.

[29] Laesecke, A., Krauss, R., Stephan, K., and Wagner, W., "Transport Properties of Fluid Oxygen," *Journal of Physical and Chemical Reference Data*, Vol. 19, No. 5, 1990, pp. 1089–1122.

[30] Kestin, J., Sengers, J. V., Kamgar-Parsi, B., and Levelt-Sengers, J. M. H., "Thermophysical Properties of Fluid H_2O," *Journal of Physical and Chemical Reference Data*, Vol. 13, No. 1, 1984, pp. 175–183.

[31] Hirschfelder, J. O., Curtiss, C. F., and Bird, R. B., "Molecular Theory of Gases and Liquids," Wiley, New York 1967, Chap. 7.

[32] Younglove, B. A., and Ely, J. F., "Thermophysical Properties of Fluids: Methane, Ethane, Propane, Isobutene and Normal Butane," *Journal of Physical and Chemical Reference Data*, Vol. 16, No. 4, 1987, pp. 577–798.

[33] Chung, T. H., Ajlan, M., Lee, L. L., and Starling, K. E., "Generalized Multiparameter Corresponding State Correlation for Polyatomic, Polar Fluid Transport Properties," *Industrial and Chemical Engineering Research*, Vol. 27, No. 4, 1988, pp. 671–679.